Research article
doi.org/10.1002/elsa.202100091

Chemistry Europe
European Chemical Societies Publishing

Received: 20 May 2021
Revised: 20 July 2021
Accepted: 30 July 2021

Porous polyimide separator promotes uniform lithium plating for lithium-free cells

Jui-Yu Pai[1,2] | **Hao-Yu Ku**[1] | **Chun-Cheng Lin**[1] | **Chien-Wei Chiang**[1] | **Laurence J. Hardwick**[2] | **Chi-Chang Hu**[1]

[1] Department of Chemical Engineering, National Tsing Hua University, Hsinchu, Taiwan

[2] Department of Chemistry, Stephenson Institute for Renewable EnergyUniversity of Liverpool, Liverpool, UK

Correspondence
Chi-Chang Hu, Department of Chemical Engineering, National Tsing Hua University, Hsinchu 300044, Taiwan.
Email: cchu@che.nthu.edu.tw
Laurence J. Hardwick, Department of Chemistry, Stephenson Institute for Renewable Energy, University of Liverpool, Liverpool, UK.
Email: Laurence.Hardwick@liverpool.ac.uk

Funding information
Ministry of Science and Technology (MOST) of Taiwan, Grant/Award Numbers: MOST 108-2923-E-007-001, 109-2923-E-007-005; National Tsing Hua University, Grant/Award Number: 110Q2708E1

Abstract

Electrospun polyimide (PI) separators were found to reduce the charge-transfer resistance of Li plating/stripping and the overpotentials of Li nucleation/growth onto Cu foils in the 1.2 M $LiPF_6$/(ethylene carbonate/dimethyl carbonate = 1/1) electrolyte without any additives in comparison with polyethylene (PE) separators. Lithium deposition through the PI separator led to the formation of a granular morphology of 15–30 μm in diameter compared to lithium dendrites using PE. A similar trend of lithium deposition was observed in $LiFePO_4$//Cu cells. The PI separator was found to enhance the discharge capacity and cycle life of Li plating/stripping in the Li//Cu and $LiFePO_4$//Cu cells containing 40 μl electrolytes, verifying that the PI separator provides dendrite inhibition capability for the lithium-metal-free cells.

KEYWORDS
copper substrate, dendrite inhibition, lithium plating/stripping, polyimide, separator

1 | INTRODUCTION

Electrode materials with high charge capacities have drawn wide attention.[1–4] Lithium metal is reconsidered as a favorable candidate for the negative electrode[5–7] since it shows a high theoretical capacity (3860 mAh/g) and very negative potential (–3.04 V vs. standard hydrogen electrode).[5–9] Furthermore, cells containing lithium ions in the positive electrodes with the in-situ generation of the negative metallic lithium on current collectors are expected to further boost the energy density[10–13] because of the minimum volume requirement. These cells are assembled in the lithium-metal-free state, attractive for manufacturing purposes.

The poor cycling performance due to low coulombic efficiencies and safety issues ascribed to Li dendrite formation hamper the commercial application of lithium metal cells.[6,8,11,14] In lithium metal cells, the anodic stripping usually occurs at the base of Li dendrites, leading to the generation of electronically insulated dead lithium[15] and low Li utilization. Moreover, metallic lithium was identified in the dead lithium and wrapped in the solid-electrolyte-interphase (SEI) in the outer shell. Therefore, dead lithium is not able to be utilized in the redox

Research article
doi.org/10.1002/elsa.202100091
Chemistry Europe
European Chemical Societies Publishing

reaction for charge storage,[10] deteriorating the coulombic efficiency of lithium metal cells greatly.[8,10,16]

To promote the round-trip efficiency of lithium metal cells, morphology control of lithium deposits is the most effective strategy.[8,10] The quantity of dead lithium after stripping can be reduced if Li is deposited in a compact structure with a granular morphology.[8,10] The electrodeposition of metallic lithium consists of nucleation and grain growth on current collectors[17] although the negative potential of lithium deposition generally leads to the SEI formation.[17] Accordingly, a spike nucleation overpotential is normally visible in the early stage,[17] which is closely correlated to the resultant lithium morphology[17,18] because of the inverse relationship between nuclei size and electrochemical overpotential.[17] Hence, any factors affecting the lithium deposition process would contribute to the overpotentials, probably changing the resultant morphology. Interestingly, the physical properties, for example, electrolyte uptake, ionic conductivity, wettability, etc., of electrolyte-soaked separators between two electrodes contribute to the overpotential of lithium deposition. For commercial polyethylene (PE) and polypropylene separators, the coulombic efficiency of lithium metal batteries (LMBs) utilizing the common $LiPF_6$-based electrolytes is normally unacceptable,[10] and modifications of separators have been proposed.[19–21] These studies indicate that separator is a significant factor determining the morphology of Li deposits. Therefore, designing separators with desirable properties can enhance the round-trip efficiencies of LMBs.

Herein, a highly porous electrospun polyimide (PI) separator with controllable thickness and high electrolyte wettability was prepared to fundamentally investigate the pure influences of separators on the Li plating/stripping performance. In comparison with the commercial PE separator, the superior wettability of electrospun PI facilitates the uniform lithium-ion flux, resulting in larger and granular lithium deposition. The high ionic conductivity and wettability of PI also decrease the overpotential of lithium deposition to obtain a Li deposit with a dense, granular morphology.[22–24] The good contact between the copper current collector and the wettable PI nanofibres absorbed with electrolyte may further improve the electrolyte affinity to the copper surface, decreasing the energy barrier required for lithium nucleation, leading to the uniform lithium deposition. The uniform and granular lithium deposition facilitate the stripping process, leading to higher discharge capacities for both Li//Cu and $LiFePO_4$//Cu cells even though the coulombic efficiencies of the PI-cells studied here were low in comparison with the literature values (>97%) which were obtained from the electrolytes containing fluoroethylene carbonate (FEC), $LiNO_3$, or other additives. Furthermore, the electrolyte employed in this work contained a slightly over-concentrated LP30 without any additives to investigate the pure influences from the separators.

2 | EXPERIMENTAL SECTION

2.1 | Materials

Pyromellitic dianhydride and 4,4-oxydianiline were purchased from Echo Chemical Co. (Taiwan). Dimethylformamide and polyvinylpyrrolidone (PVP, Mw = 1300000) were obtained from Sigma Aldrich Co. (USA). The PE membrane with a thickness of 25 μm from Asahi Chemicals was used as a commercial separator for comparison purposes. The 1.2 M $LiPF_6$ electrolyte used for Li//Cu and $LiPF_6$//Cu was a mixture from 1 M $LiPF_6$ and 2 M $LiPF_6$ mixed carbonated solutions (ethylene carbonate/dimethyl carbonate, EC/DMC = 1/1) purchased from Sigma Aldrich Co. All reactants were analytical grade.

2.2 | Fabrication of polyimide nanofibres

Polyamic acid solutions were prepared from reacting pyromellitic dianhydride and 4,4-oxydianiline in an equivalent molar ratio at 25°C for 12 h. The total mass of the solution (including polymer and solvent) prepared for the electrospinning process is 5.7 g, which contains 0.8 g polyamic acid and 0.2 g PVP. Accordingly, the total concentration of polymers in the solution is about 17 wt.% and PVP in the polymers is 20 wt.%. After the polymer solution was stirred for 12 h, it was transferred to a syringe and pushed at a flow rate of 0.3-0.5 mL/h under a voltage of 13–16 kV during the electrospinning process. The as-prepared fabrics were heated in an oven at 300°C for 2 h to transform the polyamic acid fabrics into the PI membranes. The PE and PI membranes were shaped into circles 16 mm in diameter as the separators for the cell testing.

2.3 | Separator characterization

The surface morphology and fiber diameters were observed with scanning electron microscopy (SEM, Hitachi S-4200). The pores size distribution was measured by a capillary flow porometer (PMI Inc.). The porosity of separators was estimated according to the following equation:[25]

$$P\ (\%) = \frac{\frac{M_{BuOH}}{\rho_{BuOH}}}{\frac{M_{BuOH}}{\rho_{BuOH}} + \frac{M_P}{\rho_P}} \times 100\% \quad (1)$$

where M_P and M_{BuOH} are the mass of a dry separator and the one soaked in *n*-butanol for 2 h, respectively. The electrolyte uptake was conducted by the same method but replace *n*-butanol with the electrolytes and plug the weight in the following equation:[26]

$$\text{Electrolyte uptake} = \frac{W_1 - W_0}{W_0} \times 100\% \quad (2)$$

where W_0 and W_1 are the mass of dried and soaked separators, respectively. The conductivity of separators was measured by an electrochemical system (CHI600, CHI instrument, USA) using the electrochemical impedance spectroscopic (EIS) method under the open-circuit state with an alternating current (AC) amplitude of 10 mV from 1 to 100 kHz. The configuration of the Swagelok cell was a sandwich structure with two stainless steel (304) on both sides. The conductivity of soaked separators was estimated through the following equation:[27]

$$\sigma = \frac{d}{R_b \times A} \quad (3)$$

where R_b is the bulk resistance obtained from the EIS data in the high-frequency end, d and A are the thickness and area of separators. The 1.2 M $LiPF_6$ (EC/DMC) electrolyte was also used to measure the static contact angle by means of a commercial drop shape system (First Ten Angstrom Co.).

The linear sweep voltammetry was conducted to determine the potential window of various separators in a Swagelok cell where the lithium metal was a reference electrode and stainless steel was the counter electrode. The interfacial resistance between lithium metal and electrolyte was measured by the EIS method but lithium metal was employed as electrodes on both sides to estimate the charge-transfer resistance. The cell tests for Li//Cu and $LiFePO_4$//Cu were examined using a coin-type cell (CR2032). The volume of electrolytes used for each cell was fixed to be 40 µl. The water contents of both electrolytes were confirmed to be below 5 ppm determined by the Karl Fisher titration (KF Coulometer, Metrohm Ag. Co., Switzerland). The $LiFePO_4$ electrodes purchased from Ubiq Tech. Co., Taiwan were ready-to-use commercial products coated onto the Al current collectors. The mass loading of $LiFePO_4$ is 11.52 mg/cm^2 and the capacity is 140 mAh/g (discharged at 1 C) obtained by battery testing equipment (Land CT2001A, China). For the cycle performance test, the $LiFePO_4$//Cu was charged and discharged at 0.1 C for the first cycle and then, charged at 0.2 C and discharged at 0.5 C. The cell voltage window for the above charge-discharge test was between 2.5 and 4 V. For Li//Cu, the cycle performance was conducted by a WBCS3000L battery test system (WonATech, Korea) at 1 mA/cm^2. The area capacity for Li plating/stripping is 1 mAh/cm^2. The maximum voltage for stripping was 1 V. When the cell voltage of Li//Cu reaches 1 V during the stripping step, the cell voltage is kept at 1 V to wait for reaching the time to switch the plating program. After the charge-discharge cycling tests, the separators were taken out, rinsed with the carbonate solvent for observing the morphology of separators by SEM.

TABLE 1 Physical characteristics of polyimide (PI) and polyethylene (PE) separators

Electrolyte	1.2 M $LiPF_6$ in EC/DMC = 1/1 (volume)	
Type of separator	polyimide	polyethylene
Thickness (µm)	25	25
Porosity (%)	>95	70
Electrolyte uptake (%)	2700	141
Conductivity (mS/cm)	1.22	0.55
MacMullin number	7.77	17.25

Abbreviation: EC/DMC, ethylene carbonate/dimethyl carbonate

3 | RESULTS AND DISCUSSION

3.1 | Basic properties of separators

The surface morphologies of PE and PI separators are presented in Figures 1a,b, respectively. From a comparison of Figure 1, the porosity and pore size of the PE separator are much lower and smaller than those of the PI film. These results are consistent with the pore size distribution and porosity data shown in Table 1. Additionally, the average pore sizes of the PE and PI separators, obtained from Figures 1c,d, are approximately equal to 0.03 and 0.4 µm in diameter, respectively. The pore size of electrospun PI separators is much higher than that of PE ones, probably enhancing the ionic conductivity. Moreover, the high porosity of such PI separators with great electrolyte affinity results in high electrolyte uptake presented in Table 1. The high electrolyte affinity of PI also enables to bring sufficient amounts of electrolyte to the copper surface and makes the even ion distribution, leading to deposit lithium uniformly.[19,28,29] Figures 1e,f show the results of the thermo-dimensional stability test for both PI and PE separators examined in an oven heated at 150°C for 1 h. The PI separator remained in its original shape after the above test, however, the PE separator experienced significant shrinkage, revealing the excellent thermo-dimensional stability of the PI separator. The excellent thermo-dimensional stability of PI separators

Research article
doi.org/10.1002/elsa.202100091
Chemistry Europe
European Chemical Societies Publishing

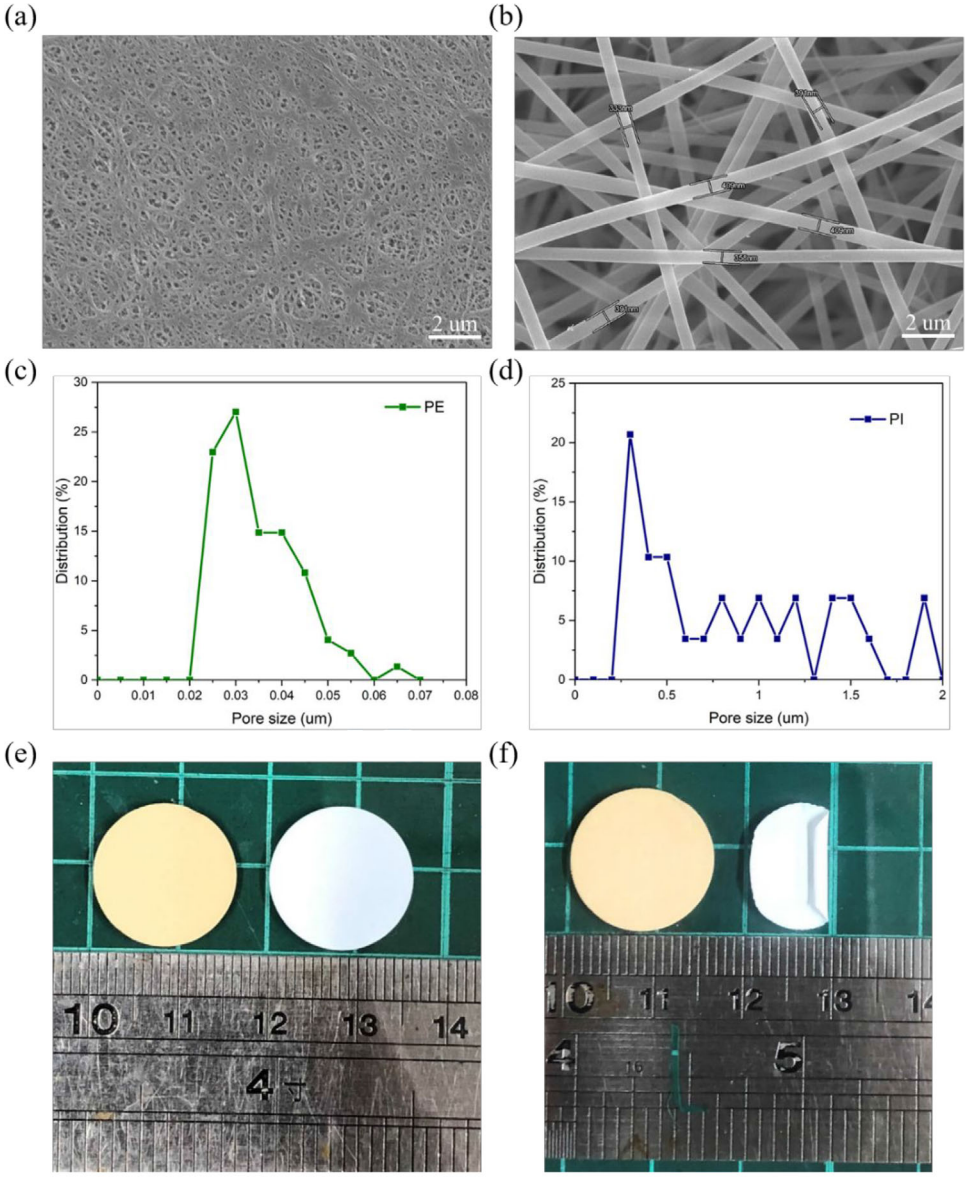

FIGURE 1 (a, b) Scanning electron microscopy (SEM) images and (c, d) the pore distribution of (a, c) polyethylene (PE) and (b, d) polyimide (PI) separators. (e, f) The photographs of (left) PI and (right) PE separators (e) before and (f) after the thermal shrinkage test (heated at the 150°C for 1 h)

has also been reported previously,[24,30–32] which is understandable since PI was transformed from polyamic acid through annealing at 300°C for 2 h.

The basic physical properties of PE and PI separators are presented in Table 1. To have a fair comparison, the thickness of PI and PE separators is the same. In Table 1, the porosity of the electrospun PI film is 25% higher than that of a PE separator. In addition, the electrolyte uptake of PI separators is approximately 2700%, which is around 2500% higher than that of PE separators. This result is understandable because the PI separator can provide lots of space to accommodate the electrolyte. Furthermore, the ionic conductivity of the PI separator is approximately 2.2 times that of the PE film, indicating that the PI separators enable to facilitate the even ionic flow, resulting in the granular, uniform lithium deposition.[19,28,29]

The 1.2 M $LiPF_6$ (EC/DMC) electrolyte was also used to measure the static contact angle of separators by means of a commercial drop shape system (First Ten Angstrom Co.) and the results are shown in Figure 2. Clearly, the PI separator can absorb the electrolyte quickly and be wetted completely. This indicates the good electrolyte affinity of PI, which facilitates the even distribution of lithium ions, alleviating the tip effect and favoring the bumpy morphology of metallic Li deposited evenly on the copper surface.[19,28,29,33]

Research article
doi.org/10.1002/elsa.202100091
Chemistry Europe
European Chemical Societies Publishing

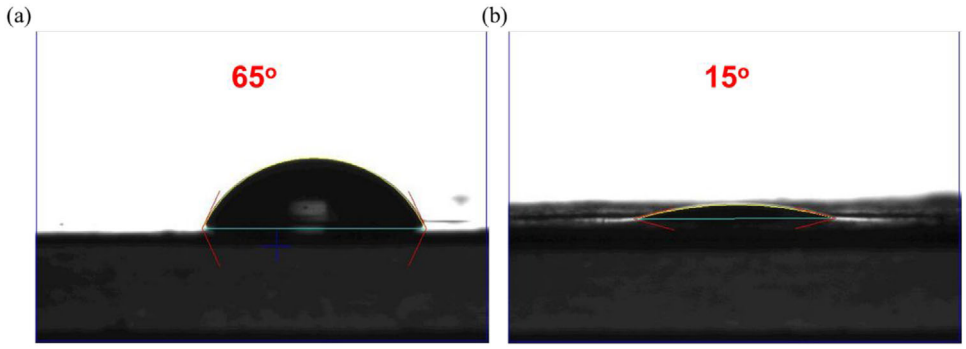

FIGURE 2 The static contact angle images of polyethylene (PE) (a) and polyimide (PI) (b) with 1.2 M $LiPF_6$ in ethylene carbonate/dimethyl carbonate (EC/DMC) = 1/1

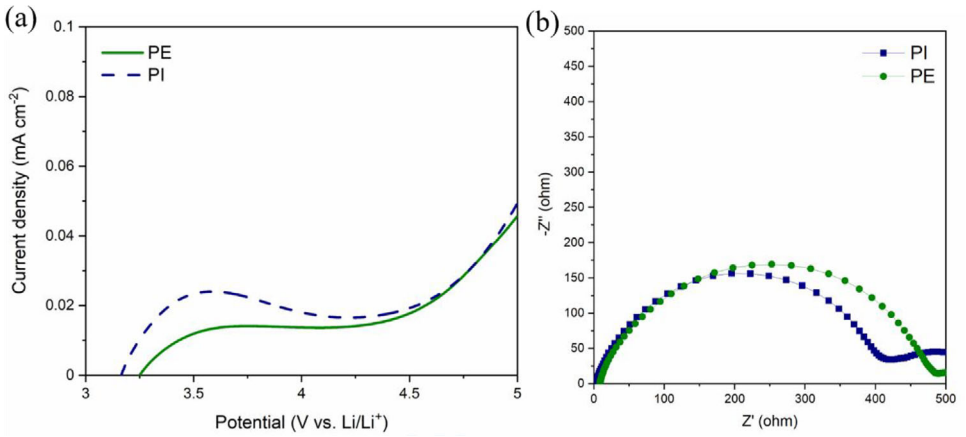

FIGURE 3 (a) Linear sweep voltammetry (LSV) curves from 3 to 5 V at 10 mV/s for Li/separator/stainless steel (SS) coin cells and (b) the Nyquist plots of Li/separator/Li coin cells in 1.2 M $LiPF_6$ (ethylene carbonate/dimethyl carbonate [EC/DMC] = 1/1) with (–, ■) polyimide (PI) and (–, ●) polyethylene (PE) separators

3.2 | Electrochemical properties of PE and PI separators

Figure 3a reveals that both separators soaked with electrolytes are electrochemically stable in the potential windows below 4.5 V (vs. Li^+/Li) since the cells employing both separators kept in the background current responses (<0.025 mA/cm^2) when the cell voltages were below 4.5 V. The current densities are always lower than 0.05 mA/cm^2 (i.e., only a little increment) when the cell voltage was scanned from 4.5 to 5.0 V. This slight increase in the linear sweep voltammetry current response may be attributed to the reactions among stainless steel electrodes, electrolytes, and separators.

From Figure 3b, the charge-transfer resistance of Li stripping/plating under the open circuit potential in 1.2 M $LiPF_6$ (EC/DMC = 1/1) for the cell using the PI separator was 423 ± 5 Ω which is lower than that for the cell using the PE separator (488 ± 5 Ω). Therefore, polyimide could decrease the overpotential of Li stripping/plating, favoring the growth of large, dense lithium deposits rather than lithium dendrites.[17] Furthermore, the low resistance is of benefits to the ion transportation at high current densities, leading to uniform lithium-ion flux.[19,28] This phenomenon also facilitates the uniform lithium deposition and promotes the reversibility of Li plating/stripping, showing the promising application potential to both lithium metal cells and Li-free cells.

Figure 4a presents the voltage profiles of Li deposition at 0.5 mA/cm^2 on copper in Li//Cu cells employing PE and PI separators. The difference in the initial sharp peak potentials is 40 mV, revealing that polyimide can decrease the Li nucleation overpotential and favors the growth of large, dense lithium deposits. The cell voltage gradually decreased in the above 2-h deposition process when the cell voltage passed the nucleation overpotential, implying that lithium atoms prefer to grow upon the existing nuclei rather than nucleation. Furthermore, the lateral growth of

Research article
doi.org/10.1002/elsa.202100091
Chemistry Europe
European Chemical Societies Publishing

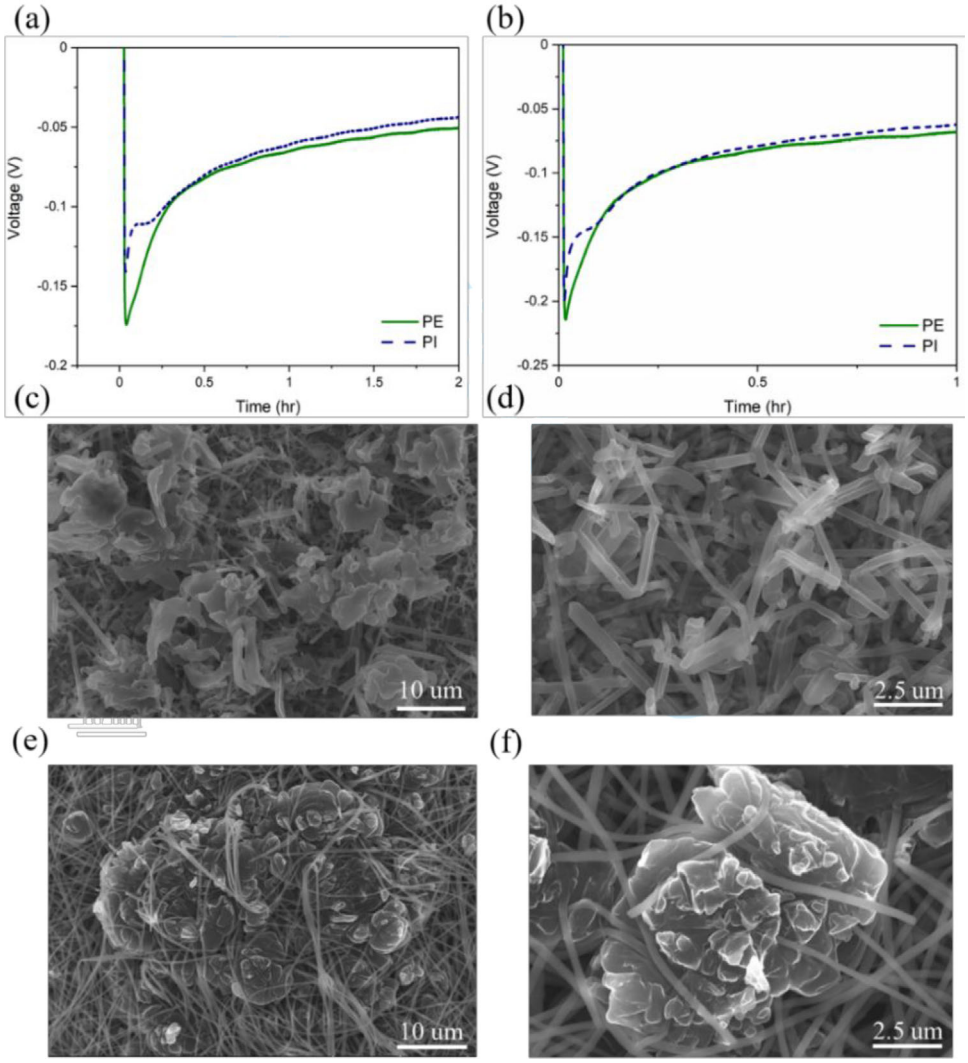

FIGURE 4 (a, b) The voltage profiles of Li deposition in Li//Cu cells at (a) 0.5 and (b) 1.0 mA/cm^2 in 1.2 M $LiPF_6$ (ethylene carbonate/dimethyl carbonate [EC/DMC] = 1/1) with (–) polyimide (PI) and (—) polyethylene (PE) separators. (c–f) Scanning electron microscopy (SEM) morphologies of Li deposits plated at (c, e) 0.5 and (d, f) 1 mA/cm^2 in Li//Cu cells using (c, d) PE and (e, f) PI separators

Li grains to form a uniform lithium deposit may cause a monotonous decrease in the cell voltage since Li-ions are continuously supplied from the Li electrode. Interestingly, throughout the whole deposition period, the voltages in the absolute value for the cell employing the PI separator are always smaller than those for the cell using the PE separator (e.g., at the end of Li deposition, –50 and –43 mV for the cells using PE and PI separators, respectively). Similar trends are also visible when the deposition current density is changed from 0.5 to 1.0 mA/cm^2 (Figure 4b), that is, the nucleation voltages equal to –213 and –199 mV, and the voltages at the end of deposition equal to –68 and –62 mV for the cells using PE and PI separators, respectively. All these results reveal that the overpotentials of Li nucleation and growth on Cu can be reduced by the PI separator.

The SEM images for the surface morphology of Li deposits on Cu shown in Figures 4c–f match well with the above results that the PI separator favors the growth of large, dense lithium grains on Cu foils because of the reduced overpotential of Li deposition resulting from the high electrolyte wettability of PI.[17,19,28,29] Hence, the metallic lithium deposited on Cu presents the grain morphology (Figure 4e) in the cell employing the PI separator rather than the dendrite lithium (Figure 4c) in the cell using the PE separator. The results obtained at 1 mA/cm^2 show similar trends to those measured at 0.5 mA/cm^2. However, the Li dendrites are more apparent because of the complete coverage of Li dendrites on the Cu substrate from Figure 4d while large agglomerates consisting of lithium grains are visible in Figure 4f. The granular morphology can alleviate the dead lithium formation[34,35] and requires less amount of electrolyte to form a stable SEI layer,[35,36] beneficial to the round-trip coulombic efficiency of cells.[35,37] Therefore, PI separators favor lithium

Research article
doi.org/10.1002/elsa.202100091
Chemistry Europe
European Chemical Societies Publishing

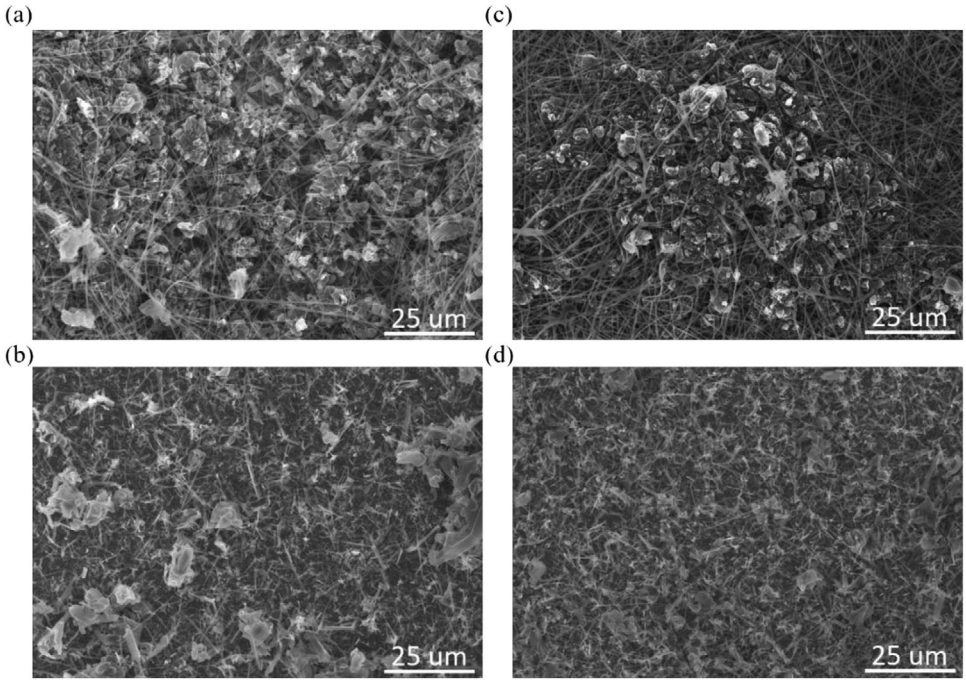

FIGURE 5 Scanning electron microscopy (SEM) morphologies of Li deposits in Li//Cu cells using (b, d) polyethylene (PE) and (a, c) polyimide (PI) separators at (a, b) 0.5 and (c, d) 1 mA/cm^2 at a low magnification

stripping/plating on Cu, suitable for lithium-metal-free cells (e.g., $LiFePO_4$//Cu). Note the long wires visible in Figures 4e,f, which are the electrospun PI fibers.

The SEM images at low magnification for the metallic lithium deposited on the copper surface are shown in Figure 5 which demonstrates that the cell using a PI separator can deposit granular lithium at both 0.5 and 1 mA/cm^2. The size distributions and the average particle sizes of granular Li obtained at 0.5 and 1 mA/cm^2 are equal to ca. 8.5 and 4.6 μm (analyzed by Image J software which is presented in Figure S1), respectively. By contrast, there are a lot of lithium dendrites formed at both current densities in the cells using the PE separator even though a few pieces of massive lithium are deposited on the copper surface. Furthermore, the average diameters of Li dendrites (analyzed by Image J software) are approximately 1.0 and 0.3 μm when the current densities of deposition are equal to 0.5 and 1 mA/cm^2, respectively.

There may be a doubt that the reduction in the charge-transfer resistance and overpotentials of Li deposition and growth can be related to the electrolyte uptake and/or pore size of the separator. The high electrolyte uptake of a separator generally results from the electrolyte affinity of the separator polymer and the separator porosity. On the other hand, in this work, the electrolyte volume in all coin cell tests was fixed to be 40 μl. Consequently, the cells using the PI separator did not contain more electrolytes than those using the PE separator. Therefore, the electrolyte uptake is not the main factor reducing the charge-transfer resistance of Li deposition. The porosity concern is also clarified by the data shown in Figure S2 of the Supporting Information where a cured electrospun polyacrylonitrile separator with high porosity but relatively poor electrolyte affinity cannot improve the Li plating/stripping performance in comparison with the PI separator. Accordingly, the electrolyte affinity of the separator polymer is the key factor affecting the charge-transfer resistance and overpotentials of Li deposition and growth, leading to the variation in the morphology of Li deposits.

Figure 6a compares the charge-discharge voltage profiles of Li//Cu cells using PE and PI separators at 1 mA/cm^2 with an area capacity of 1 mAh/cm^2. Initially, the coulombic efficiencies of both cells are similar (90% and 93% for PE and PI separators, respectively) but continuously decline with cycling. At the 100th cycle, the cell using the PI separator shows better charge-discharge performances from the lower overpotential of Li plating and the higher stripping capacity in comparison with the cell using the PE separator. In addition, the stripping capacity of the cell using the PI separator is much higher than that of the cell using a PE separator although the plating capacity for both separators is the same. This difference is attributable to the PI separator favoring the deposition of large lithium grains/agglomerates, inhibiting the formation of dead lithium after stripping. All the above results are in good agreement with the SEM images where the granular Li deposits provide higher coulombic efficiencies of lithium stripping/plating than the dendritic Li deposits.[8]

Research article
doi.org/10.1002/elsa.202100091
Chemistry Europe
European Chemical Societies Publishing

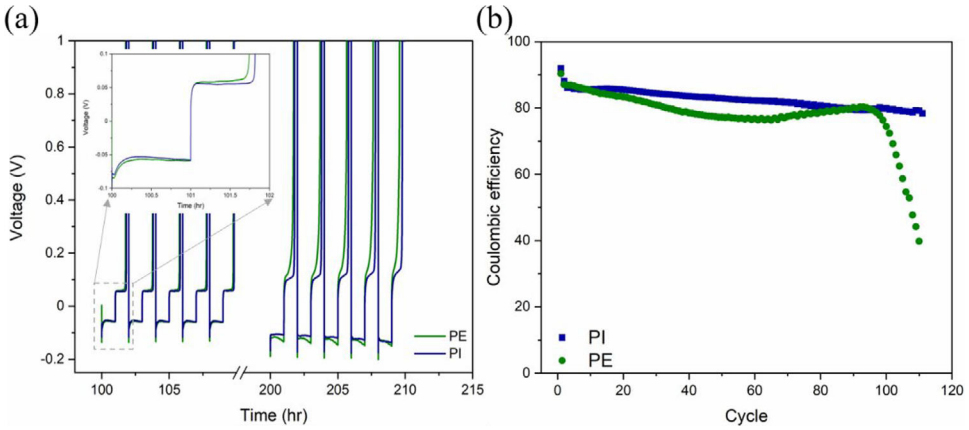

FIGURE 6 (a) The voltage profile and (b) the coulombic efficiency versus cycle number for the Li//Cu cells using (–, ■) polyimide (PI) and (—, ●) polyethylene (PE) separators measured at 1 mA/cm^2 with the Li stripping/plating capacity of 1 mAh/cm^2

The coulombic efficiency against the cycle number measured at 1 mA/cm^2 for the Li//Cu cell using PI and PE separators in 1.2 M LiPF6 (EC/DMC = 1/1) is shown in Figure 6b. The coulombic efficiency for the cell using the PE separator declines gradually from 90% to ca. 75% at the 60th cycle, then, slightly increases to 83% at the 96th cycle, and finally decays rapidly to 50% at the 110th cycle. The above slight increment in the coulombic efficiency between 60 and 96 cycles is probably attributed to the significant growth of Li dendrites into the PE separator, reducing the distance and *i*R drops between Cu and Li electrodes.[38] For the cell employing the PI separator, its coulombic efficiency experiences a gradual decrement from 93% to 80% at the 90th cycle and then keeps at this plateau afterward. Note that the coulombic efficiencies of both cells using the two separators in this study are obviously lower than those reported in the literature which introduced the additives of fluoroethylene carbonate, $LiNO_3$, KNO_3, or other compounds to obtain high coulombic efficiencies (>95%). The present study, another hand, was conducted in the absence of such additives in order to investigate the only impact of the separator on the reversibility of Li plating/stripping, i.e., using only a common electrolyte.

Figure 7a demonstrates the 1st, 10th, and 20th charge-discharge voltage profiles of two $LiFePO_4$//Cu cells in 1.2 M $LiPF_6$ (EC/DMC = 1/1). The initial discharge capacity of the PI-cell is 128 mAh/g, in comparison to the PE-cell (100 mAh/g), even though the charge capacities of both cells obtained in the first charge cycle are around 150 mAh/g. This result reveals that PI separators increase the redox reversibility of deposited lithium in full cells. Additionally, the difference in discharge capacity for the PE- and PI-cells was noticeable during the initial 10 cycles (e.g., 50 and 66 mAh/g at the 10th cycle). Due to the limited Li^+ in such Li-metal-free cells, the discharge capacity of the PI-cell was reduced to 20 mAh/g at the 20th cycle although the discharge capacity of the PI-cell is always higher than that of the PE-cell from Figure 7b. Therefore, PI separators do improve the reversibility of Li plating/stripping, reasonably resulting from its large grains with a granular morphology. Note that the rate capability for the cells using PE and PI separators was also examined and found that the cells using PI separators exhibited higher discharge capacities at any specified cycle or current density in comparison with the cell using PE separators (Figures S3 and S4). From both figures, the initial discharge capacities of cells using PI separators were ca. 140 mAh/g which is much higher than those of the cells using PE ones (about 100 mAh/g) at 0.1 C. In addition, the above discharge capacity gap is always visible in the following galvanostatic charge-discharge (GCD) cycles measured at various current densities. All the above results suggest that PI separators favor the uniform deposition of lithium on Cu and facilitate the discharge capacity of the lithium metal-free cells.

The morphologies of lithium deposits on copper in $LiFePO_4$//Cu cells using PE and PI separators are presented in Figures 7c,d, respectively. From these SEM images, the PI-cell can deposit granular lithium (10–15 μm) rather than dendritic lithium from the PE-cell. In addition, based on the analysis of these SEM images at low magnification from Figures 7e,f (by Image J software), the average particle size of granular lithium formed in the PI-cell is approximately 8 μm, which is 4.5 μm larger than the lithium deposited in the PE-cell (Figure S5). These results matching well with the data from the Li//Cu cells reveal that the low overpotentials of lithium nucleation/deposition in the PI-cell favor the growth of granular, large grains/agglomerates. Therefore, PI separators can improve the cycle performance of lithium-metal-free cells because the morphology of lithium deposits was

Research article
doi.org/10.1002/elsa.202100091
Chemistry Europe
European Chemical Societies Publishing

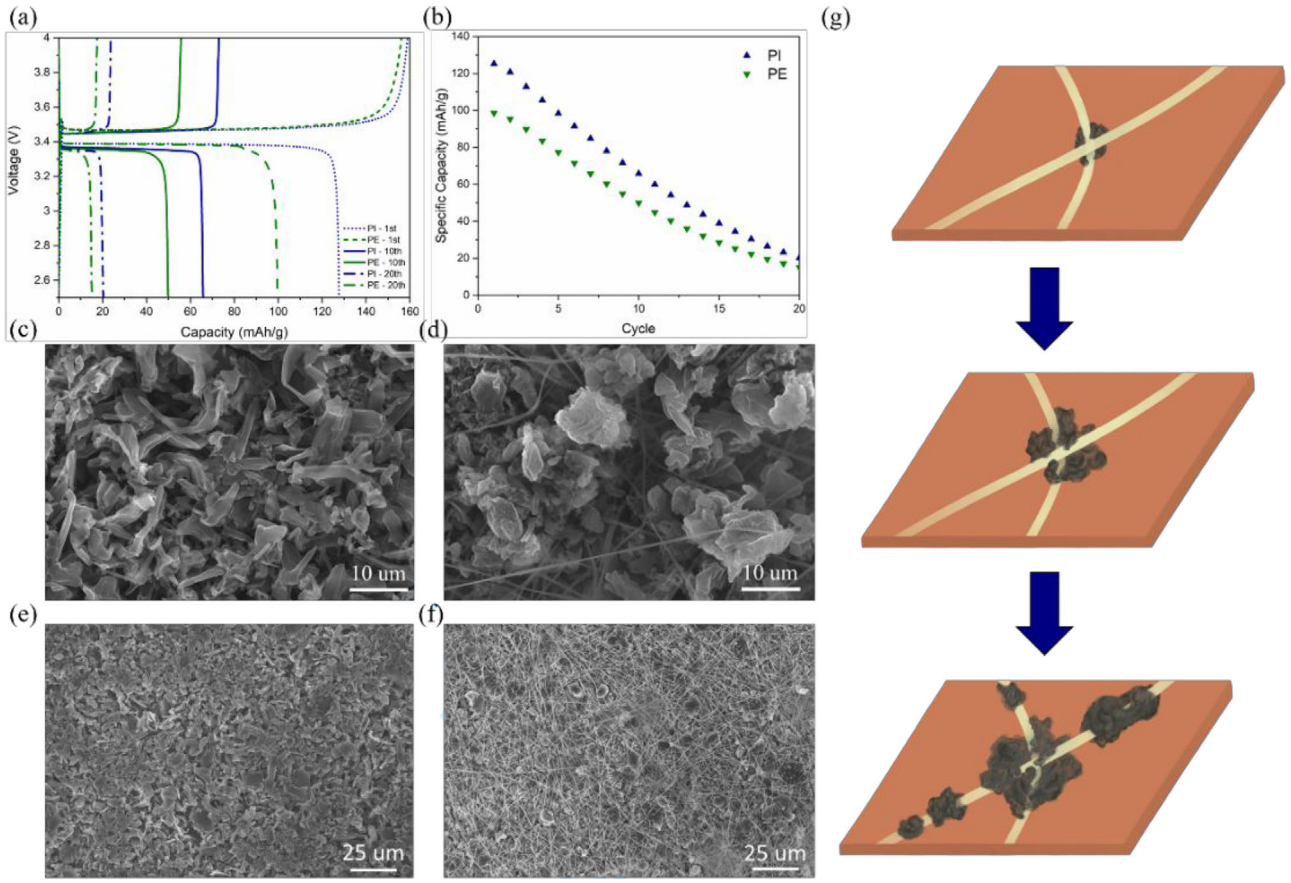

FIGURE 7 (a) The 1st, 10th, and 20th charge-discharge profiles for the $LiFePO_4$//Cu cells with polyethylene (PE) and polyimide (PI) separators. (b) Specific capacity against cycle number for $LiFePO_4$//Cu cells with (▼) PE and (▲) PI separators. (c–f) Scanning electron microscopy (SEM) images of Li deposits on copper at 0.1 C for the $LiFePO_4$//Cu cells using (c, e) PE and (d, f) PI separators after the first half charging cycle. (g) The scheme of Li deposition at the PI fibers/Cu interface

confirmed to be a crucial factor influencing the coulombic efficiency.[8,10]

Figure 7g illustrates the schematic diagram of lithium deposition on the copper surface. The reduced overpotential of lithium deposition observed for the cell using the PI separator, resulting in the granular Li morphology, is attributable to the high compatibility of PI with carbon-based electrolytes because of its functional groups (e.g., aromatic C–N and C=O). These functional groups decrease the charge-transfer resistance of Li deposition to alleviate the dendrite formation. The good contact between copper and PI fibers with these wettable functional groups absorbing vast amounts of electrolyte is believed to improve the electrolyte affinity to the copper surface, leading to the reduced charge-transfer resistance of Li plating/stripping. Accordingly, Li deposition favorably occurs at the interface between PI fibers and copper, resulting in the growth of Li grains surrounding the PI fibers.

Figure 8 shows the morphologies of PE and PI separators from the $LiFePO_4$//Cu cell after the 20-cycle GCD test and the Li//Cu cells after the 120-cycles GCD test at 0.5 and 1 mA/cm^2, respectively. Note that all the separators were taken out from the coin cells, rinsed with the pure carbonate solvents to remove electrolyte residues. Clearly, the morphologies of the PI separators were not significantly changed after the GCD cycling test. However, a lot of pores in the PE separator taken out from the Li//Cu cells after the 120-cycle GCD test at 1 mA/cm^2 were distorted and partially clogged with certain species although the other two cases do not show this separator degradation.

4 | CONCLUSIONS

The impact of the type of separator polymers on the redox reversibility of Li plating/stripping on Cu foils in 1.2 M $LiPF_6$ (EC/DMC = 1/1) electrolyte without any electrolyte additives has been shown. The PI separators are of benefit to the improvement in the discharge capacity and the lithium plating/stripping reversibility of the Li-ion-limited $LiFePO_4$//Cu cells. The PI separator with high

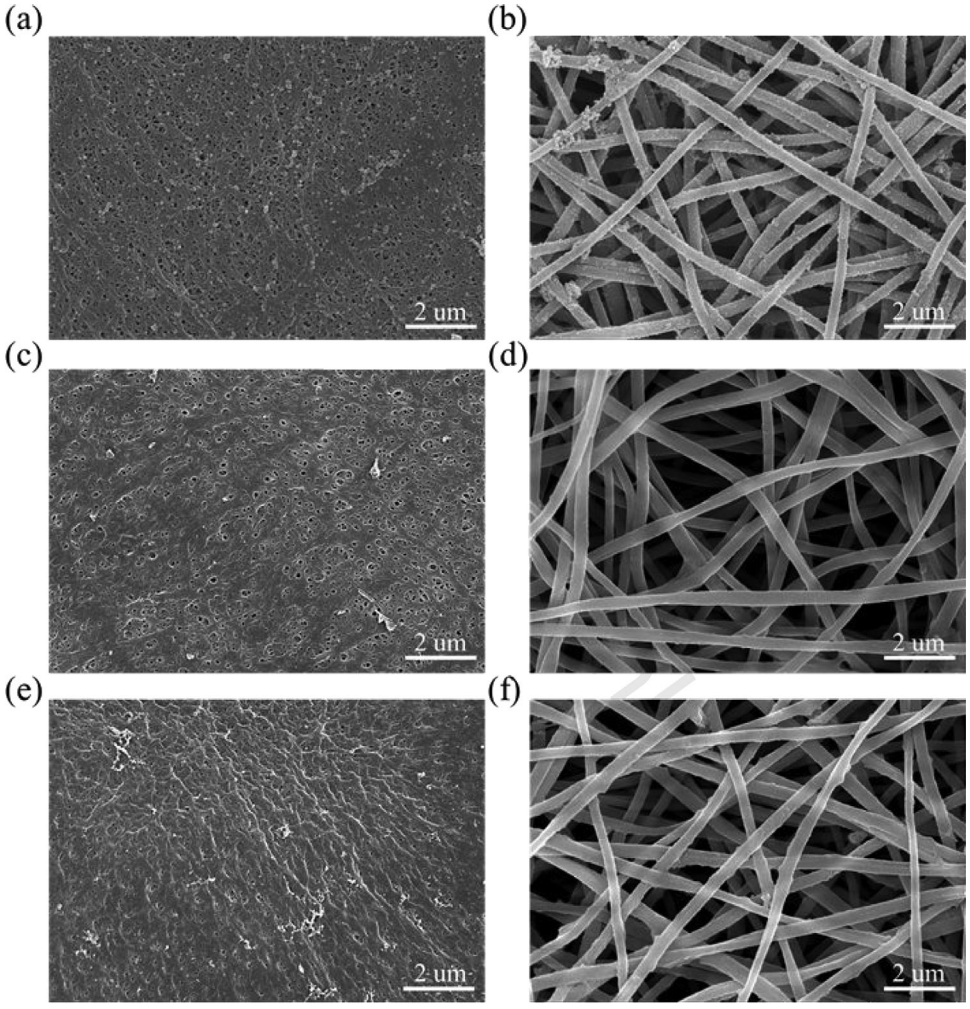

FIGURE 8 Scanning electron microscopy (SEM) images of polyethylene (PE) (a, c, e) and polyimide (PI) (b, d, f) separators after cycling. The $LiFePO_4$//Cu cells are shown in (a) and (b). The Li//Cu cells at the 0.5 and 1 mA/cm^2 are presented in (c, d) and (e, f), respectively

compatibility with the carbonate electrolytes significantly improves the ionic conductivity, distributes the electrolyte uniformly, and reduces the charge-transfer resistance, significantly reducing the nucleation and plating overpotentials to form the granular-like lithium deposit on the copper foil to enhance the lithium reversibility and cycle life of Li plating/stripping. Therefore, the Li//Cu cell using the PI separator with 40 μl electrolyte but no additives can maintain the coulombic efficiency higher than 80% for more than 100 cycles.

ACKNOWLEDGMENTS

The financial support of this work, by the Ministry of Science and Technology (MOST) of Taiwan under contract no. MOST 108-2923-E-007-001, 109-2923-E-007-005, and National Tsing Hua University under contract no. 110Q2708E1 is gratefully acknowledged.

DATA AVAILABILITY STATEMENT

Data included in the article supporting information, or on request.

REFERENCES

1. L. Ji, Z. Lin, M. Alcoutlabi, X. Zhang, *Energy Environ. Sci.* **2011**, *4*, 2682.
2. F. Yang, H. Gao, J. Hao, S. Zhang, P. Li, Y. Liu, J. Chen, Z. Guo, *Adv. Funct. Mater.* **2019**, *29*, 1808291.
3. J. Lu, Z. Chen, F. Pan, Y. Cui, K. Amine, *Electrochem. Energy Rev.* **2018**, *1*, 35.
4. J. Hassoun, B. Scrosati, *J. Electrochem. Soc.* **2015**, *162*, A2582.
5. J. Liu, Z. Bao, Y. Cui, E. J. Dufek, J. B. Goodenough, P. Khalifah, Q. Li, B. Y. Liaw, P. Liu, A. Manthiram, *Nat. Energy* **2019**, *4*, 180.
6. Q. Li, S. Zhu, Y. Lu, *Adv. Funct. Mater.* **2017**, *27*, 1606422.
7. C. Yang, K. Fu, Y. Zhang, E. Hitz, L. Hu, *Adv. Mater.* **2017**, *29*, 1701169.
8. C. Fang, J. Li, M. Zhang, Y. Zhang, F. Yang, J. Z. Lee, M.-H. Lee, J. Alvarado, M. A. Schroeder, Y. Yang, *Nature* **2019**, *572*, 511.

9. C. Jin, O. Sheng, J. Luo, H. Yuan, C. Fang, W. Zhang, H. Huang, Y. Gan, Y. Xia, C. Liang, *Nano Energy* **2017**, *37*, 177.
10. J. Zheng, M. S. Kim, Z. Tu, S. Choudhury, T. Tang, L. A. Archer, *Chem. Soc. Rev.* **2020**, *49*, 2701.
11. J. Qian, B. D. Adams, J. Zheng, W. Xu, W. A. Henderson, J. Wang, M. E. Bowden, S. Xu, J. Hu, J. G. Zhang, *Adv. Funct. Mater.* **2016**, *26*, 7094.
12. A. A. Assegie, J.-H. Cheng, L.-M. Kuo, W.-N. Su, B.-J. Hwang, *Nanoscale* **2018**, *10*, 6125.
13. V. Pande, V. Viswanathan, *ACS Energy Lett.* **2019**, *4*, 2952.
14. X. Q. Zhang, X. Chen, X. B. Cheng, B. Q. Li, X. Shen, C. Yan, J. Q. Huang, Q. Zhang, *Angew. Chem.* **2018**, *130*, 5399.
15. K.-H. Chen, K. N. Wood, E. Kazyak, W. S. LePage, A. L. Davis, A. J. Sanchez, N. P. Dasgupta, *J. Mater. Chem. A* **2017**, *5*, 11671.
16. F. Sun, I. Manke, *ChemElectroChem* **2019**, *6*, 5787.
17. A. Pei, G. Zheng, F. Shi, Y. Li, Y. Cui, *Nano Lett.*. **2017**, *17*, 1132.
18. C. Wei, H. Fei, Y. An, Y. Tao, J. Feng, Y. Qian, *J. Mater. Chem. A* **2019**, *7*, 18861.
19. R. Pan, X. Xu, R. Sun, Z. Wang, J. Lindh, K. Edström, M. Strømme, L. Nyholm, *Small* **2018**, *14*, 1704371.
20. W.-K. Shin, A. G. Kannan, D.-W. Kim, *ACS Appl. Mater. Interfaces* **2015**, *7*, 23700.
21. H. Huo, X. Li, Y. Chen, J. Liang, S. Deng, X. Gao, K. Doyle-Davis, R. Li, X. Guo, Y. Shen, *Energy Storage Mater.* **2020**, *29*, 361.
22. Y. Li, Q. Li, Z. Tan, *J. Power Sources* **2019**, *443*, 227262.
23. Y.-E. Miao, G.-N. Zhu, H. Hou, Y.-Y. Xia, T. Liu, *J. Power Sources* **2013**, *226*, 82.
24. C.-T. Hsieh, S.-C. Lin, C.-H. Lee, C.-F. Liu, C.-C. Hu, *J. Electrochem. Soc.* **2019**, *166*, A3132.
25. L. Kong, B. Liu, J. Ding, X. Yan, G. Tian, S. Qi, D. Wu, *J. Membr. Sci.* **2018**, *549*, 244.
26. F. Zhang, X. Ma, C. Cao, J. Li, Y. Zhu, *J. Power Sources* **2014**, *251*, 423.
27. Y. Liang, S. Cheng, J. Zhao, C. Zhang, S. Sun, N. Zhou, Y. Qiu, X. Zhang, *J. Power Sources* **2013**, *240*, 204.
28. S. Ryu, T. Sugimoto, J. Kim, K. Park, D. Im, Y.-G. Lee, J. W. Choi, *ACS Appl. Energy Mater.* **2021**, *4*, 5237.
29. F. Shen, K. Wang, Y. Yin, L. Shi, D. Zeng, X. Han, *J. Mater. Chem. A* **2020**, *8*, 6183.
30. Z. Zhou, T. Zhao, X. Lu, H. Cao, X. Zha, Z. Zhou, *J. Power Sources* **2018**, *396*, 542.
31. C.-E. Lin, H. Zhang, Y.-Z. Song, Y. Zhang, J.-J. Yuan, B.-K. Zhu, *J. Mater. Chem. A* **2018**, *6*, 991.
32. C. Shi, P. Zhang, S. Huang, X. He, P. Yang, D. Wu, D. Sun, J. Zhao, *J. Power Sources* **2015**, *298*, 158.
33. X. B. Cheng, T. Z. Hou, R. Zhang, H. J. Peng, C. Z. Zhao, J. Q. Huang, Q. Zhang, *Adv. Mater.* **2016**, *28*, 2888.
34. X. Q. Zhang, X. B. Cheng, X. Chen, C. Yan, Q. Zhang, *Adv. Funct. Mater.* **2017**, *27*, 1605989.
35. K. Shen, Z. Wang, X. Bi, Y. Ying, D. Zhang, C. Jin, G. Hou, H. Cao, L. Wu, G. Zheng, *Adv. Energy Mater.* **2019**, *9*, 1900260.
36. N. W. Li, Y. X. Yin, C. P. Yang, Y. G. Guo, *Adv. Mater.* **2016**, *28*, 1853.
37. B. L. Mehdi, A. Stevens, J. Qian, C. Park, W. Xu, W. A. Henderson, J.-G. Zhang, K. T. Mueller, N. D. Browning, *Sci. Rep.* **2016**, *6*, 34267.
38. Y. Cheng, L. Zhang, S. Xu, H. Zhang, B. Ren, T. Li, S. Zhang, *J. Mater. Chem. A* **2018**, *6*, 18479.

SUPPORTING INFORMATION

Additional supporting information may be found in the online version of the article at the publisher's website.

How to cite this article: J.-Y. Pai, H.-Y. Ku, C.-C. Lin, C.-W. Chiang, L. J. Hardwick, C.-C. Hu, *Electrochem. Sci. Adv.* **2021**, e2100091. https://doi.org/10.1002/elsa.202100091